Applied Energy 161 (2016) 349–363

Contents lists available at ScienceDirect

Applied Energy

journal homepage: www.elsevier.com/locate/apenergy

Particle-filtering-based estimation of maximum available power state in Lithium-Ion batteries

Claudio Burgos-Mellado [a], Marcos E. Orchard [a,*], Mehrdad Kazerani [b], Roberto Cárdenas [a], Doris Sáez [a]

[a] Department of Electrical Engineering, Faculty of Mathematical and Physical Sciences, University of Chile (DIE), Av. Tupper 2007, 8370451 Santiago, Chile
[b] Department of Electrical and Computer Engineering, University of Waterloo, 200 University Avenue West, Waterloo, Ontario, Canada

HIGHLIGHTS

- Approach to estimate the state of maximum power available in Lithium-Ion battery.
- Optimisation problem is formulated on the basis of a non-linear dynamic model.
- Solutions of the optimisation problem are functions of state of charge estimates.
- State of charge estimates computed using particle filter algorithms.

GRAPHICAL ABSTRACT

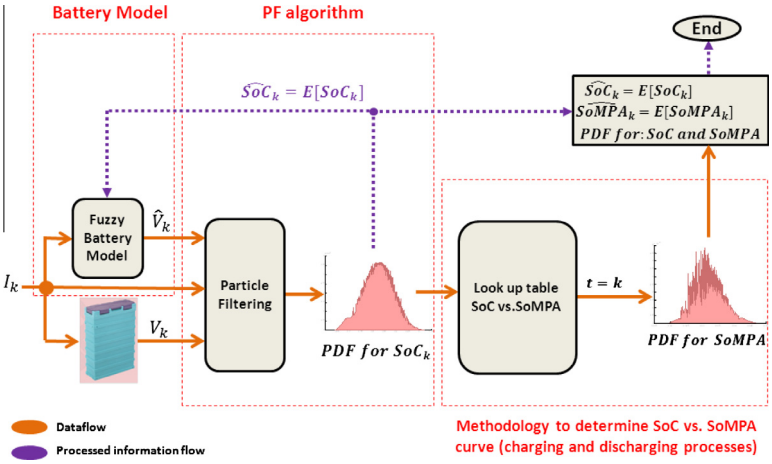

ARTICLE INFO

Article history:
Received 19 May 2015
Received in revised form 12 September 2015
Accepted 20 September 2015

Keywords:
State of maximum power available
Lithium-Ion battery
Nonlinear dynamic model
State estimation
Particle filtering

ABSTRACT

Battery Energy Storage Systems (BESS) are important for applications related to both microgrids and electric vehicles. If BESS are used as the main energy source, then it is required to include adequate procedures for the estimation of critical variables such as the State of Charge (SoC) and the State of Health (SoH) in the design of Battery Management Systems (BMS). Furthermore, in applications where batteries are exposed to high charge and discharge rates it is also desirable to estimate the State of Maximum Power Available (SoMPA). In this regard, this paper presents a novel approach to the estimation of SoMPA in Lithium-Ion batteries. This method formulates an optimisation problem for the battery power based on a non-linear dynamic model, where the resulting solutions are functions of the SoC. In the battery model, the polarisation resistance is modelled using fuzzy rules that are function of both SoC and the discharge (charge) current. Particle filtering algorithms are used as an online estimation technique, mainly because these algorithms allow approximating the probability density functions of the SoC and SoMPA even in the case of non-Gaussian sources of uncertainty. The proposed method for SoMPA estimation is validated using the experimental data obtained from an experimental setup designed for charging and discharging the Lithium-Ion batteries.

* Corresponding author.
E-mail address: morchard@ing.uchile.cl (M.E. Orchard).

http://dx.doi.org/10.1016/j.apenergy.2015.09.092
0306-2619/

Nomenclature

C_n	nominal capacity
I	battery current
I^*	feasible points
I_s	operational current limit given by the manufacturer (120 A for both charging and discharging processes)
I^C_{max}	maximum current at charging period
I^D_{max}	maximum current at discharging period
η	coulombic efficiency
R_{int}	internal resistance
T_s	sampling period
V	battery terminal voltage
V_s	operational voltage limit given by the manufacturer (28.6 V for charging process and 22.4 V for discharging process)

List of acronyms

AEKF	adaptive extended Kalman filter
BESS	Battery Energy Storage Systems
BEVs	battery electric vehicles
BMS	Battery Management Systems
DCIR	direct current internal resistance
DEKF	dual extended Kalman filter
EKF	extended Kalman filter
HEVs	hybrid electric vehicles
HPPC	hybrid pulse power characterisation
NCRE	non-conventional renewable energy
PDF	probability density function
PF	Particle Filtering
SoC	State of Charge
SoH	State of Health
SoMPA	State of Maximum Power Available
SOA	Safe Operating Area
Voc	open circuit voltage

1. Introduction

In recent years the interest in environmental protection and energy sustainability has steadily increased; this fact has promoted research activities and projects focused on non-conventional renewable energy (NCRE) sources as a replacement for fossil fuels [1–4]. In this context, the concepts of hybrid electric vehicles (HEVs), battery electric vehicles (BEVs), and solar automobiles are nowadays commonly found in electro-mobility companies. Battery Energy Storage Systems (BESSs) are of paramount importance in the technologies where they fulfil the role of principal energy source. In this regard, Lithium-Ion battery banks have been widely used in electro-mobility applications due to of their high energy density and excellent cycling performance [5–7]. For the management of this sort of battery banks is important to use suitable Battery Management Systems (BMS), which consists of both dedicated hardware and software, with the purpose of providing monitoring, diagnosis, control, and estimation of relevant parameters of the battery and improving the system reliability. Important parameters related to battery banks are: State of Charge (SoC), State of Health (SoH) and State of Maximum Power Available (SoMPA). The first is associated with vehicle autonomy, the second provides information to the driver about the necessity of replacing an old or damaged battery bank. In the case of electric (or hybrid) vehicle applications, the third parameter, SoMPA, is useful for both (i) the driver when he/she has to decide how to meet requirements in terms of acceleration, regenerative braking, and gradient climbing power (without fear of over-charging or over-discharging the battery) [8,9], and (ii) the automotive companies for optimal design of the battery banks in terms of power [10,11].

The SoMPA can be defined as the maximum power that is possible to draw from or inject to the battery bank at a specific operating point without violating the Safe Operating Area (SOA). This zone is determined by temperature, current, voltage, and SoC limits, which are usually provided by the battery manufacturer in order to ensure a safe battery operation [8,10,12]. The SoMPA cannot be directly measured in a battery-based storage system; this parameter must be inferred from the observation of other

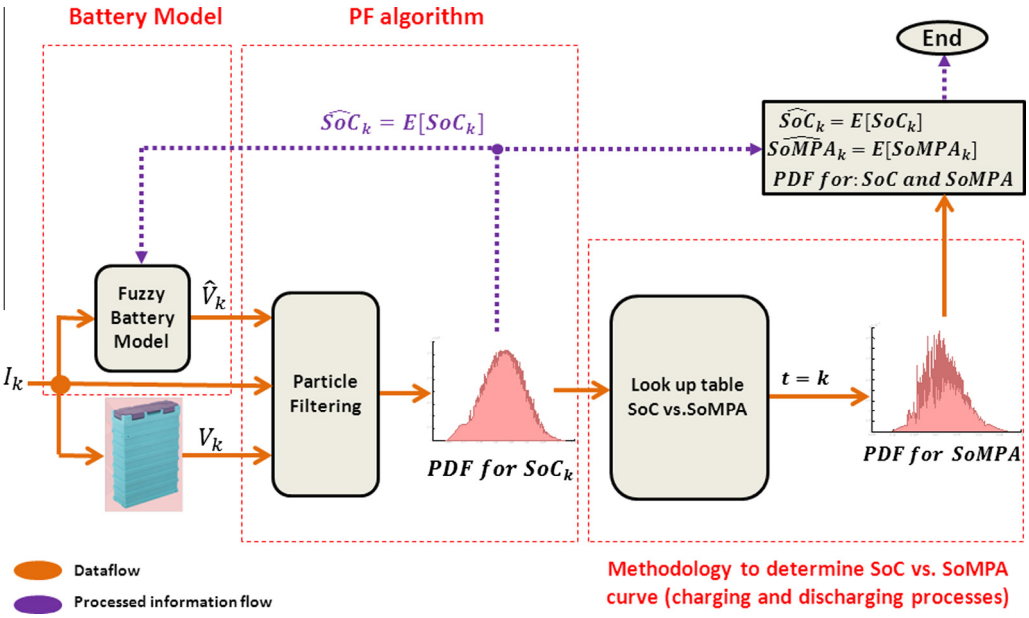

Fig. 1. The proposed SoC and SoMPA estimation scheme.

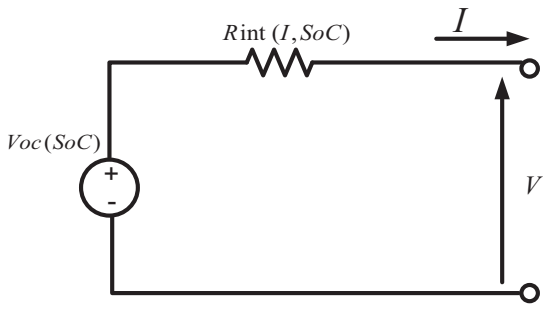

Fig. 2. Equivalent Circuit Diagram used for the development of the Fuzzy Model.

variables such as temperature, SoC and SoH [13,14]. Therefore, this work focuses on the problem of estimating the SoMPA in a Lithium-Ion battery bank during charging and discharging processes, where SoMPA represents the maximum power that may be maintained constant during the time interval $[k, k+T_s]$, where k is the present time and T_s corresponds to the sampling period, based on the present battery condition and without violating the preset operational design limits on the battery current, voltage, SoC, or power. In this particular research effort, which considers a nonlinear discrete-time battery model, this quantity may be interpreted as the maximum instantaneous power that can be extracted from (or injected to) the battery during each sampling period (T_s = 1 s). It must be noted that both SoC and SoH should be also estimated, and thus a scheme of SoMPA estimation necessarily requires the implementation of additional estimators for these two variables. Although there are number of aspects that have to be considered when estimating SoMPA, this paper will solely focus on: (i) the development of an SoMPA estimator framework that will use the SoC as an input, (ii) the development of a SoC estimator, and (iii) the use of a battery model to include polarisation effects as a function of both the SoC and the discharge/charge current.

In terms of SoC estimation, there exists a wide range of methods that can be implemented, and have been summarized in [15]. In particular, for electro-mobility systems, current research efforts are mostly focused on the development of SoC estimation algorithms based on electric models in conjunction with techniques based on fuzzy logic [16,17], neural networks [18], or Bayesian approaches such as the Extended Kalman Filter (EKF) [19–21] and Particle Filtering (PF) [22,23].

The techniques for SoMPA estimation can be divided in two groups: (i) methods based on a characteristic map, and (ii) methods based on a dynamic battery model [8]. The first category includes all the methods where mapping of the SoMPA as a function of the battery states is realised. This map is stored in the BMS memory and is used for SoMPA estimation. It must be noted that the experimental points for the generation of this map must be obtained in a controlled environment, following the recommendations proposed by some standards and regulations, as for instance (i) the hybrid pulse power characterisation (HPPC) method proposed by the Idaho National Engineering & Environmental Laboratory [24,25], and (ii) the direct current internal resistance (DCIR) method proposed by the Advanced Battery Development Center and Hitachi Research Laboratory [26]. The main advantage of characteristic map-based methods is their simplicity, while the main disadvantages are: limited adaptive capacity, static modelling of battery, and higher requirements of memory storage [8]. The second group of SoMPA estimation techniques includes all the methods that use a dynamic battery model in their estimation/prediction algorithms [8]. These methods are the most promising approaches due to their high adaptation capabilities. Basically, the main difference among the methods that could be grouped in the second category is the type of battery model that is used. In the following, the main research efforts concerning this particular topic are presented.

Table 1
Feasible points in optimisation problems.

Feasible points	Constraints	KKT Constraints
$I^* = I_s$	$\mu_1 > 0$ and $\mu_2 = \mu_3 = 0$	Satisfied
$I^* = 0$	$\mu_2 > 0$ and $\mu_1 = \mu_3 = 0$	Not satisfied
$I^* = \mp\frac{V_s - Voc(SoC)}{R_{int}}$ • Minus sign: discharging • Plus sign: charging	$\mu_3 > 0$ and $\mu_1 = \mu_2 = 0$	Satisfied

The most common approach used for SoMPA estimation is reported in [24]. The proposed method consists of determining, at each time instant, the maximum current during both charging and discharging processes. This procedure is based on a simple battery model and operational design voltage limits (V_{max}, V_{min}). The instantaneous SoMPA is computed using only the instantaneous maximum current (charging or discharging) multiplied by the operational design voltage limits (V_{max} for charging, and V_{min} for discharging). Given that this model only considers voltage limits, and it uses an open circuit voltage (Voc) source in series with a constant internal resistance, its performance is not accurate; in fact, safety or health issues may arise due to the over/under charging and discharging of the battery bank. Other disadvantages of this method are: (i) design limits such as discharge current, SoC and power are not considered in the formulation of the estimator; (ii) the manner in which the SoMPA is computed heavily depends on the sampling period T_s; and (iii) the battery model does not

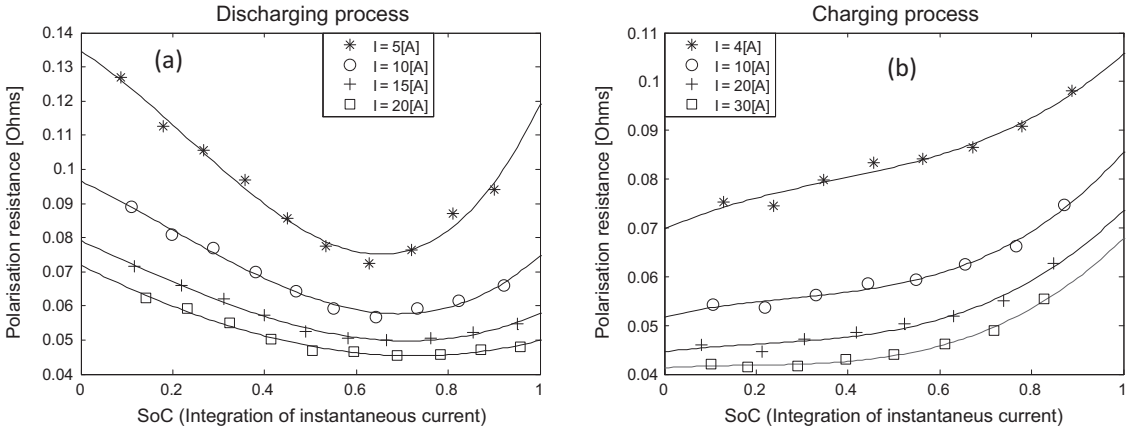

Fig. 3. Computed polarisation resistance for the discharging and charging processes.

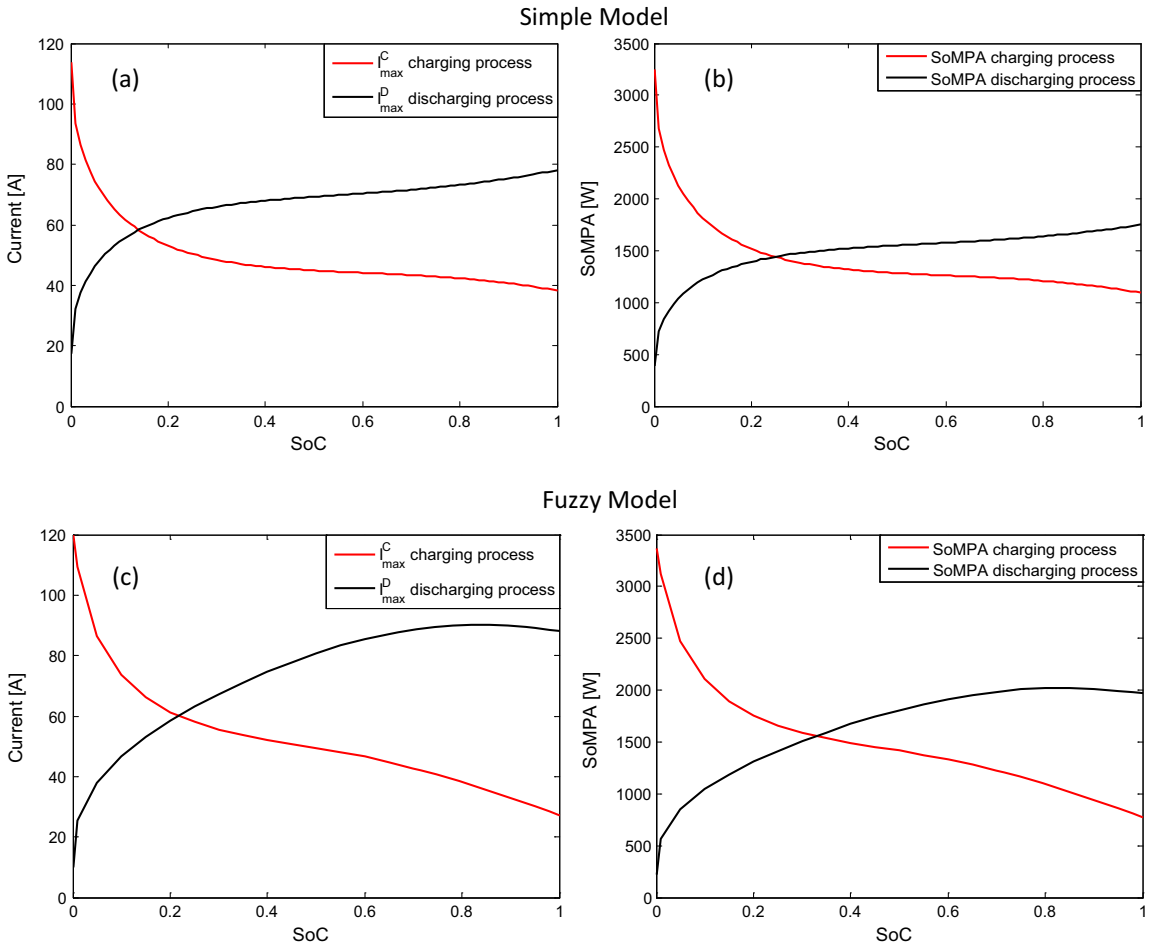

Fig. 4. (a) Solutions for the proposed optimisation problem using a simple battery model both for charging and discharging modes, (b) SoMPA as a function of the SoC in charging and discharging modes (using simple model), (c) solution of the proposed optimisation problem using fuzzy battery model in charging and discharging modes, (d) SoMPA as a function of the SoC for charging and discharging modes (using fuzzy model).

consider polarisation effects. Plett in [27] improves the aforementioned method in the following aspects: (i) design limits of current and SoC are added; (ii) the proposed method takes into account the predicted value of the SoMPA at the next sampling time. Some of the disadvantages of this method are: the battery model used is still too simplistic; it assumes a constant internal resistance; and the polarisation resistance is neglected. Also, the latter method does not consider a SoC estimation scheme (it is assumed that the SoC value is known). Sun et al. in [28] improve the Plett's method. The authors in this case take into account the polarisation effects, using a Thevenin model with one RC branch [16]. Notice that both the resistances and the capacitance are determined as a function of the SoC. The following comments can be given for this method: (i) the polarisation resistance is modelled as a function of the SoC only, even though it also depends on the current level and temperature [16,29,30]; and (ii) it does not consider the implementation of an online SoC estimation framework; in fact this is proposed as future work. Xiong et al. in [9] develop a joint estimator in order to compute both the SoC and the SoMPA in an online manner. The SoC estimator uses an Adaptive Extended Kalman filter (AEKF)-based method, while the SoMPA estimator follows a structure similar to other approaches reported in the literature [8,9,16,24,25,27–30], the only difference being that the method proposed in [9] generalizes the algorithm to sub-harmonics of the sampling frequency. Notice that both estimation algorithms are based on the one-branch Thevenin equivalent model, where the parameters are determined as a function of SoC. However, the current dependence of the polarisation resistance is not taken in account.

None of the methods described above considers the dependency of battery model parameters on the State of Health. Some research efforts have considered this dependence in an online battery model parameter identification scheme. Sun et al. in [31,32] improve their previous work [28] by developing a SoMPA estimator that uses information from an online SoC estimation module. In this work, both estimators are based on an adaptive extended Kalman filter algorithm and a Thevenin equivalent model, where an online parameter identification frame is implemented using a time-series approach. The proposed scheme was validated using experimental data and for known conditions of the battery SoH. Pei et al. in [33] proposed a SoMPA one-step ahead predictor based on a Thevenin model, using a dual extended Kalman filter (DEKF). The DEKF consists of two EKFs that run concurrently at each time instant. One of these EKFs is used to determinate Thevenin equivalent model parameters at every time step, and the other is used to estimate the discharge current in the RC branch. This approach is interesting because the algorithm is validated using experimental tests designed to obtain the actual values of the peak power. The authors in [34] proposed an improved Dynamic Matrix Control algorithm in order to linearize RC equivalent Thevenin models and predict (one-step ahead) the battery voltage. Results prove that this method is suitable and useful for predicting the voltage, and its application for SoMPA prediction is proposed as future work. Notice that none of the previous works takes into account

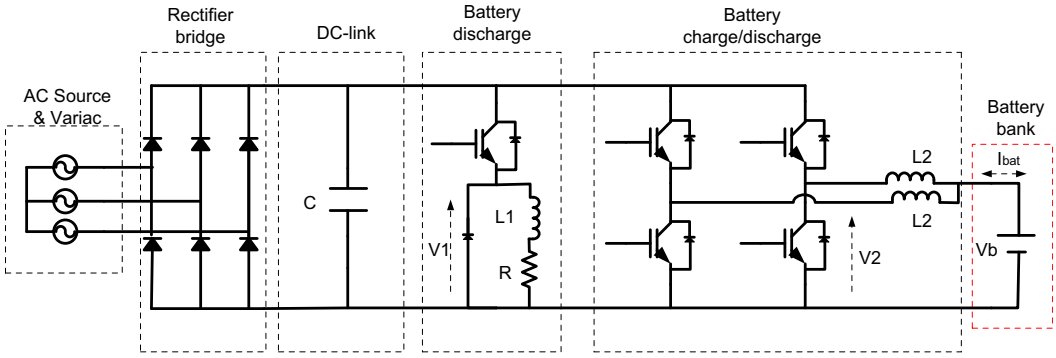

(a) Circuit Diagram

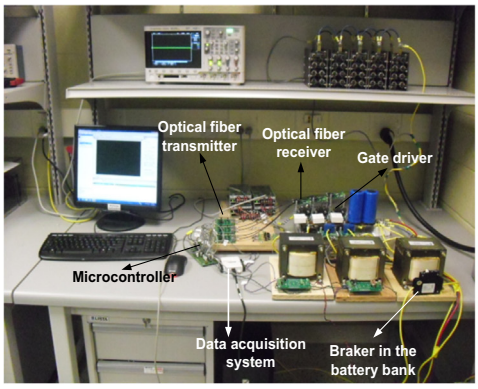

(b) Lab Prototype

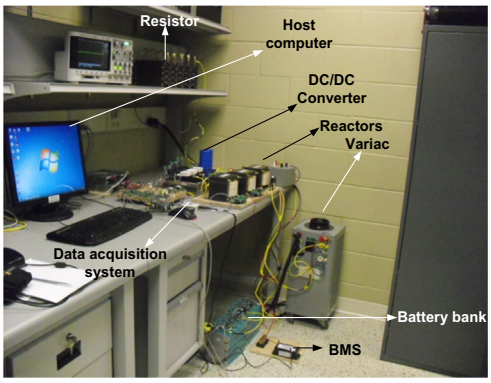

(c) Lab Prototype

Fig. 5. Experimental system.

Table 2
Theoretical solution for SoMPA based on the simplified model (19) and (20).

Discharging process	Charging process
$SoMPA(SoC_k) = -\frac{(V_s - Voc(SoC_k))}{R_{int}} \cdot V_s$	$SoMPA(SoC_k) = \frac{(V_s - Voc(SoC_k))}{R_{int}} \cdot V_s$

Table 3
Parameters of experimental system.

Nominal power	4 kW
L1	2.5 mH
L2	2.5 mH
R	1 Ω
C	6 0mF
Battery bank	8 Li-Ion cells (GBS-LFMP40Ah) in serial connection
Nominal capacity	40 AH
Nominal voltage	25.6 V
Switching frequency	10 kHz
Control platform	TMS320F2808 Texas Instruments
Data acquisition system	NI-USB-6009 National Instruments
Optical fiber transmitter	HFBR-1521Z
Optical fiber receiver	HFBR-2521Z
Current transducer	LEM LA-100P Hall-Effect transducer
Voltage transducer	LEM LV-20P Hall-Effect transducer

the polarisation resistance dependence on the battery current values and therefore these effects are not includes in the estimation modules. In this regard, Waag et al. in [8] proposed a one-step-ahead predictor of SoMPA based on an improved Thevenin equivalent model. This model represents the dependence of the polarisation resistance on the current level using an online parameter identification scheme. The disadvantage of this method is that the dependence of the polarisation resistance on the SoC is not considered.

In this work, a novel SoMPA estimator for a Lithium-Ion battery bank is proposed. As this estimator uses a nonlinear discrete-time battery model, SoMPA may be interpreted here as the maximum instantaneous power that can be extracted from (or injected to) the battery during each sampling period (T_s = 1 s). The SoMPA estimator is developed within the structure of an online SoC estimation module based on Bayesian nonlinear filtering algorithms. The schematic diagram of the proposed estimator is shown in Fig. 1. In this scheme, the SoC is estimated at each time instant based on a Particle Filtering (PF) algorithm; the PF algorithm uses the measurements of both voltage and current, while the voltage estimate is provided by a fuzzy model of the battery. The output at each time step corresponds to the probability density function (PDF) of the SoC. Then, this PDF is evaluated using a look-up table that represents the relationship between the SoC and the maximum power available. Also, the output at each time instant is a PDF for the SoMPA. Finally, the procedure to obtain the relationship between the SoC and the SoMPA requires to solve a nonlinear optimisation problem.

Three major contributions are highlighted:

- All the previous works related with SoMPA estimation assume that the maximum power available is given by the maximum available current, multiplied by operational design voltage limits. However, a mathematical proof for this assumption is missing. For this reason, in this work a mathematical formulation is developed to provide sufficient theoretical background for the computation of the SoMPA as the solution of a nonlinear optimisation problem where the SoC is an input variable.

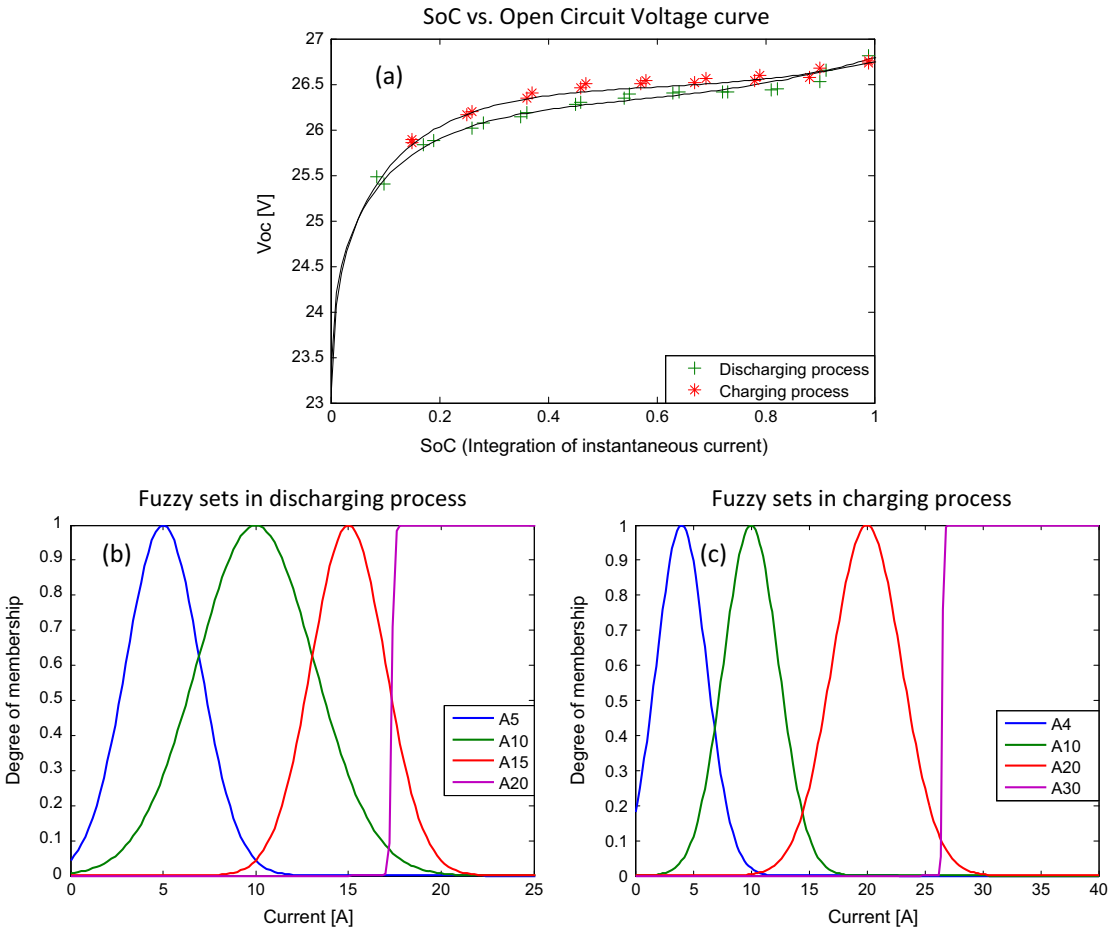

Fig. 6. (a) Voc vs. SoC curves for charging and discharging processes, (b) and (c) fuzzy sets used for fuzzy model (charging and discharging processes).

Table 4
Parameters of Voc-versus-SoC curves depicted in Fig. 6a, based on (1).

Mode	v_L	v_0	γ	α	β
Discharging	4.971	26.792	0.556	−2.631	0.508
Charging	5.033	26.750	0.556	−2.733	0.567

- The battery model used in the estimation scheme considers the dependency of the polarisation resistance on both current level and SoC.
- The proposed SoMPA estimation scheme is suitable for non-Gaussian sources of uncertainty, and the output of the module at each time instant is an empirical PDF instead of a simple expectation.

2. Theoretical background

2.1. Fuzzy battery model

A fuzzy model for the output voltage of a Lithium-Ion battery bank is described. The polarisation resistance is modelled by a non-linear interpolation (fuzzy based) of a set of available curves

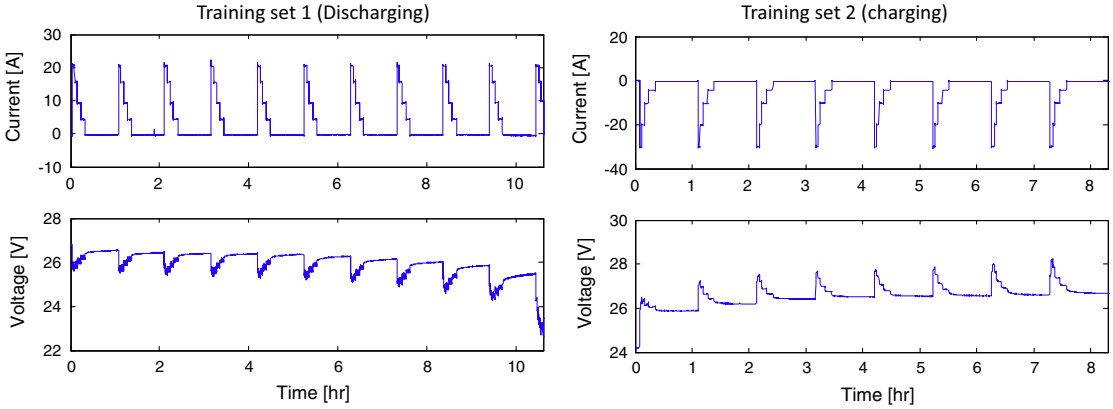

Fig. 7. Training sets.

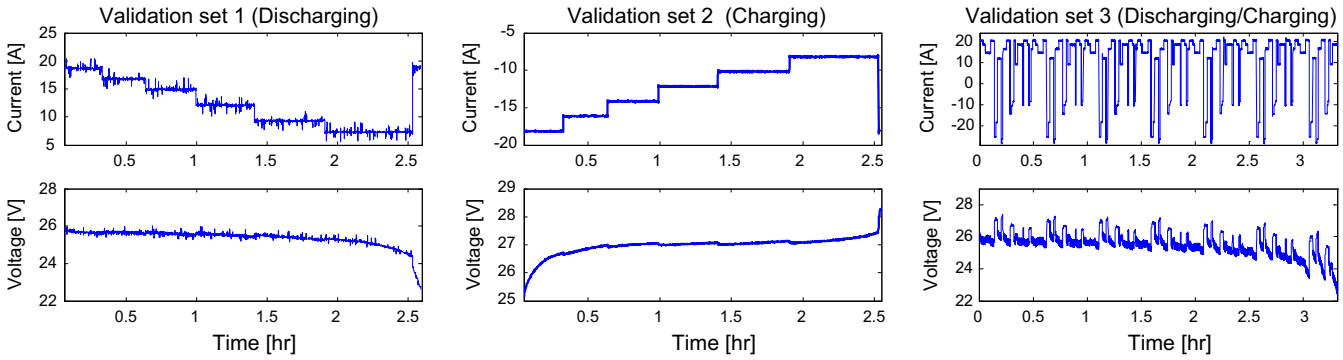

Fig. 8. Validation sets.

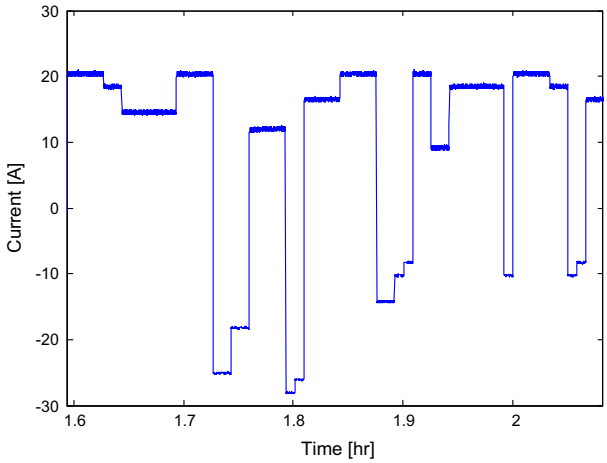

Fig. 9. Profile used in validation set #3.

Table 5
Parameters of Simple model.

	R_{int} (Ω)	RMSE
Discharge	0.0562	0.20540
Charge	0.0483	0.18326

Table 6
Parameters of Fuzzy model.

Discharge	σ_5	σ_{10}	σ_{15}	a	b	RMSE
	2.0000	3.1631	2.0000	15.9494	17.3438	0.10869
Charge	σ_4	σ_{10}	σ_{20}	a	b	RMSE
	2.1623	2.3876	3.0000	19.9748	26.5422	0.081629

Table 7
Performance indices (RMSE) for Simple and Fuzzy models using validation sets #1, #2 and #3.

	Validation set #1	Validation set #2	Validation set #3
Simple model	0.28453	0.29306	0.39797
Fuzzy model	0.16384	0.26738	0.41271

obtained experimentally at different operating points (SoC and current rates) of the battery bank.

The proposed fuzzy model is based on an equivalent circuit shown in Fig. 2, where the terminal voltage depends on the SoC, current and temperature [16]. Temperature variations are not considered in this research effort, since the battery bank was located in an environment where those variations were negligible and because the experimental setup did not include a temperature-controlled chamber that could allow validation of temperature-dependent model structures. In Fig. 2, the polarisation resistance is modelled as a non-linear function dependent on both the SoC and the charge/discharge current. It is important to note that this equivalent circuit does not consider capacitances. Thus, the polarisation voltage drop modelled by the fuzzy resistance is attributed to the ohmic resistance and static (steady-state) electrolyte polarisation; i.e., it is used mainly to describe the steady-state behaviour and low-frequency responses in the battery bank.

The source voltage $Voc(SoC_k)$ represents the open circuit voltage, which is obtained by:

$$Voc(SoC_k) = v_L + (v_0 - v_L)\cdot e^{\gamma\cdot(SoC_k-1)} + \alpha\cdot v_L(SoC_k-1) + \cdots + (1-\alpha)v_L\left(e^{-\beta} - e^{-\beta\cdot\sqrt{SoC_k}}\right). \quad (1)$$

Quantities v_L, v_0, γ, α and β are model parameters to be estimated offline according to the procedure detailed in [23]. It must be noted that the Voc curve presents hysteresis effects [35]; where the curve exhibiting higher voltage values is related to a battery charge process, while the curve that exhibits smaller voltage values is related to a battery discharge process. In real applications, the open circuit voltage could be located at any point between these charge and discharge curves [36] and, in this regard, it is important to note that this research effort does not consider these hysteresis effects in the model structure. Instead, our approach incorporates this hysteresis effect as part of model uncertainty sources that affect the evolution in time of the dynamic nonlinear system. These uncertainty sources are instantaneously quantified, and adjusted, using information that is extracted from online voltage/current measurements at battery terminals and Bayesian suboptimal filtering algorithms (see Fig. 1).

Our model also assumes noisy SoC estimates based on empirical computations based on the integral of the instantaneous current. Thus, the discrete-time model for the SoC is given by (2).

$$SoC_k = SoC_{k-1} - \eta\frac{T_s I_{k-1}}{C_n}. \quad (2)$$

In (2), C_n is the battery bank nominal capacity (34 Ah for the battery under study), T_s the sampling period (1 s in this study), I_k the current at instant k, and η the Coulombic efficiency, which is 1 in the discharging process and 0.98345 in the charging process (these values have been calculated using experimental data). Notice that I_k is considered positive for discharging current. Based on Fig. 2, the voltage at the battery terminals in discrete-time is given by:

$$V_k = Voc(SoC_k) - I_k\cdot R_{int}(SoC_k, I_k), \quad (3)$$

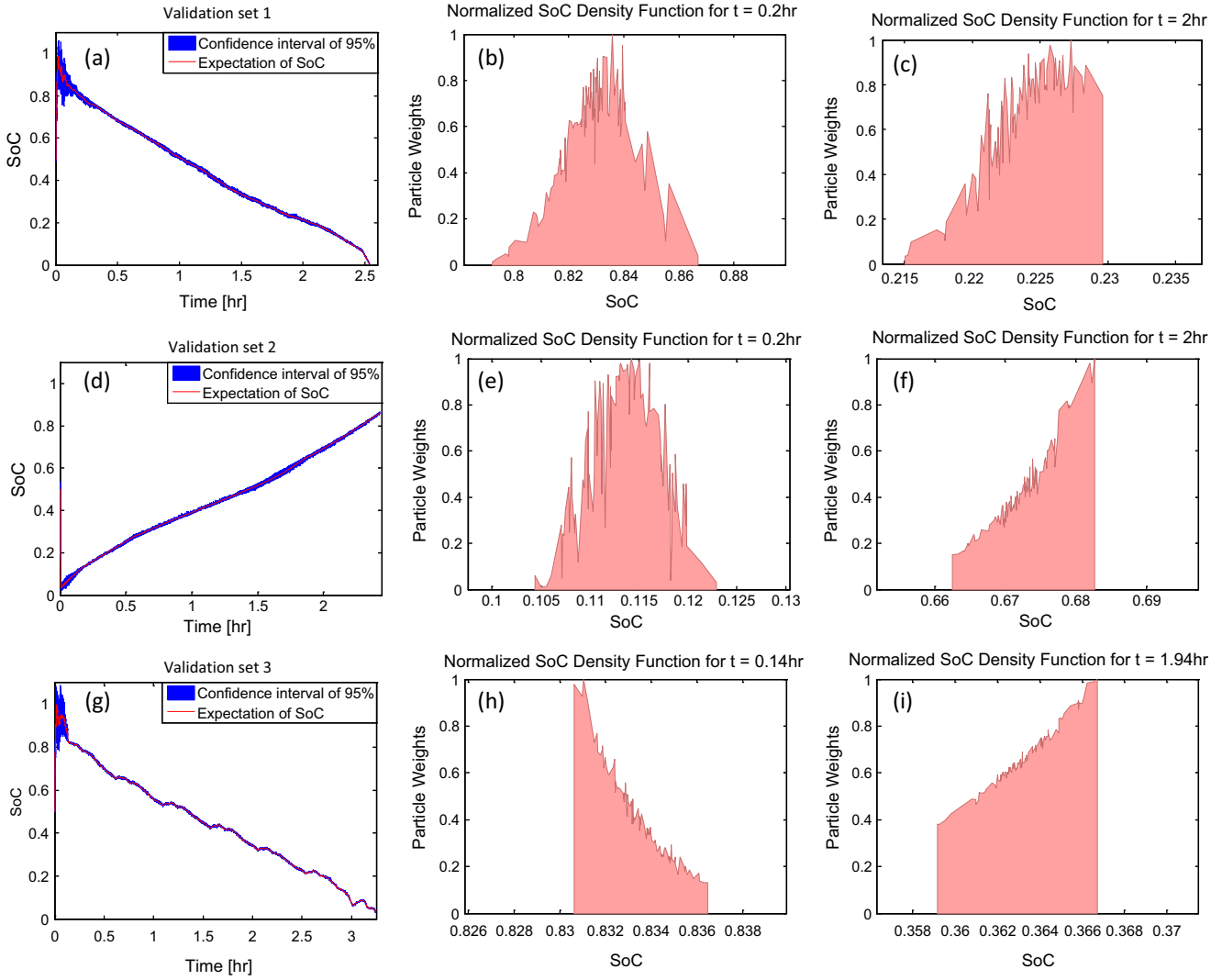

Fig. 10. Performance of the SoC estimator on validation sets.

where the voltage source $Voc(SoC_k)$ is given by (1). Then, the value of the polarisation resistance can be obtained using (3) as:

$$R_{int}(SoC_k, I_k) = \frac{Voc(SoC_k) - V_k}{I_k}. \tag{4}$$

To obtain the polarisation resistance for this model, a series of experimental tests at a number of fixed current levels were performed using the experimental system built for this work (this is further discussed in Section 4.1, "Experimental Results"). The polarisation resistance of (4) has been estimated considering experimental data obtained by charging the battery bank with current (I_k) regulated at constant values of 4 A, 10 A, 20 A and 30 A (see Fig. 3b), its corresponding voltage response (V_k) and the Voc vs. SoC curve for charging process. On the other hand, the polarisation resistance in discharging process is calculated using experimental data obtained by discharging the battery bank with current (I_k) regulated at constant values of 5 A, 10 A, 15 A and 20 A (see Fig. 3a), its corresponding voltage response (V_k), and the Voc vs. SoC curve for discharging process.

To calculate the polarisation resistance for any current in the range of operation, a fuzzy model is used to interpolate between the resistance curves for the discharging process or the curves for the charging process. Fuzzy modelling is a systematic framework for approximating a large class of non-linear systems [37,38]. The premises are based on fuzzy sets, and the consequences are non-linear or linear models that can represent different operating points of the system. The elements of the fuzzy systems belong to a discourse universe with a membership function associated with each fuzzy set. The membership function assigns a membership degree between 0 and 1 to each element of the fuzzy set. The most commonly used membership functions are triangular, trapezoidal and Gaussian shape.

In this case, the proposed fuzzy model is as follows:

$$\begin{aligned} &Rule\ j: \text{If } I_k \text{ is } A_{I_j,j} \text{ then } R_{int_j} = f_j(SoC_k), \\ &R_{int}(SoC_k, I_k) = \frac{\sum_{j=1}^{r} w_j(I_k) \cdot f_j(SoC_k)}{\sum_{j=1}^{r} w_j(I_k)} = Fuzzy(SoC_k, I_k), \end{aligned} \tag{5}$$

where w_j is the activation degree of rule j (in this case, equal to the membership degree of the fuzzy set $A_{I_j,j}$) and f_j is a non-linear function adjusted for the resistance values R_{int_j}, as a function of SoC_k at a fixed current level I_j. In this model, Gaussian membership functions are used for the fuzzy sets $A_{I_j,j}$ considering currents of 5 A, 10 A and 15 A (discharging) and 4 A, 10 A and 20 A (charging). This was inspired by the fact that each Gaussian membership function requires the tuning of only two parameters (the mean value and the standard deviation). In this particular case, the mean value of the Gaussian functions is defined as I_j, while their standard

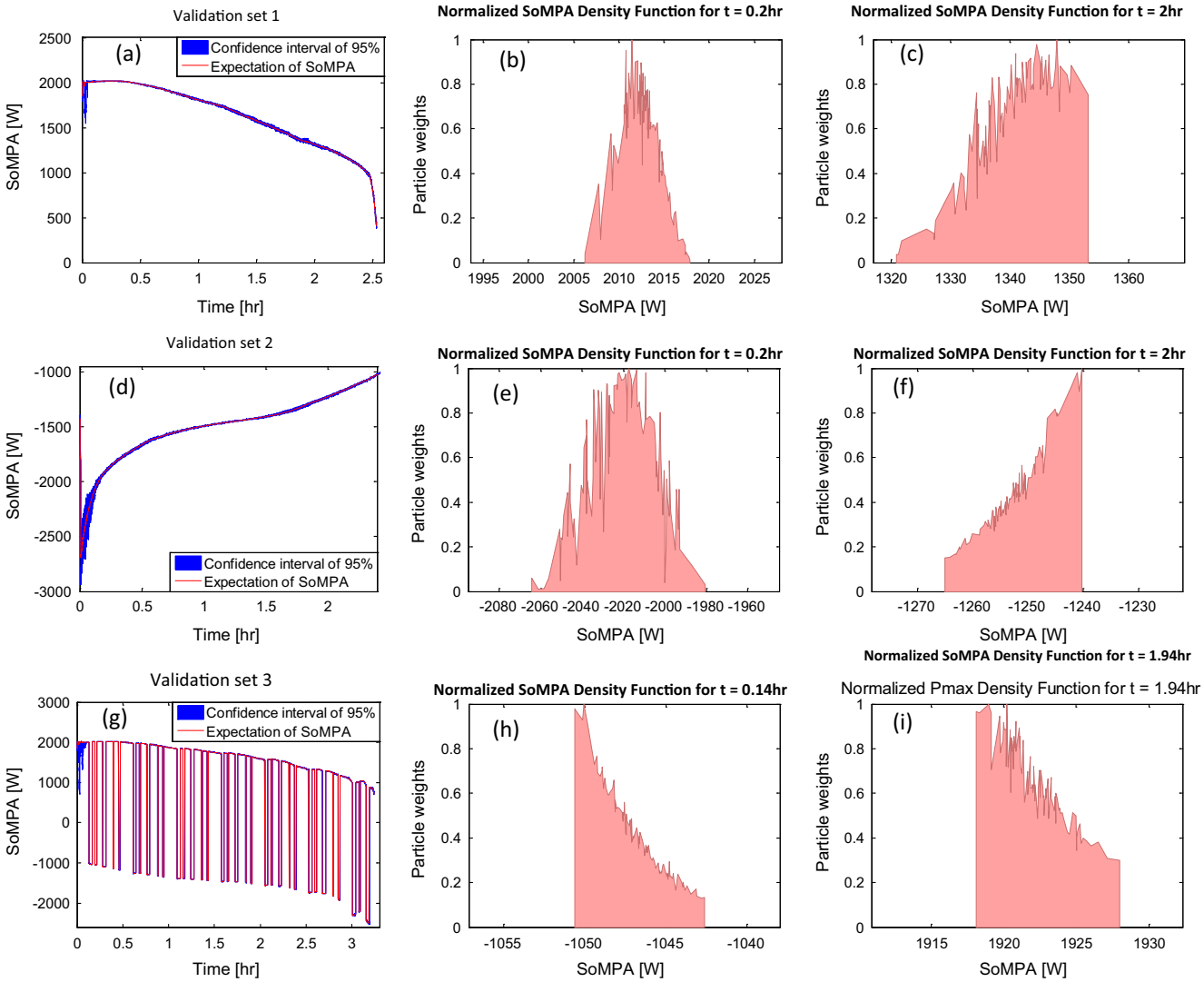

Fig. 11. Performance of the SoMPA estimator on validation sets.

deviation (σ_x) must be tuned to minimize the mean square error of the model. This minimisation problem is solved using genetic algorithms. For extreme values of currents (20 A discharging and 30 A in charging), the sigmoid functions (with parameters a, b) are used for the fuzzy sets $A_{l_j,j}$. Note that the fuzzy battery model is a multi-model, due to the fact that one model was proposed for discharging process and one for charging process. The discharge and charge models are based on the Voc vs. SoC curve represented by (1) and the polarisation resistances derived based on a fuzzy model.

Finally, it is important to mention that the performance of this model structure has been successfully validated and compared with other models that are available in the literature (such as Thevenin, Plett and Copetti models) in [16]. Provided those results, this research effort will not replicate efforts and will assume the aforementioned nonlinear fuzzy model structure to characterise the battery behaviour.

2.2. Particle-filtering-based estimator for battery state of charge

Particle Filtering (PF) are a class of algorithms designed to obtain samples from a *target* state probability distribution $\pi_k(x_{0:k})$ sequentially. These methods are aimed at generating a set of $N \gg 1$ weighted particles $\left\{w_k^{(i)}, x_{0:k}^{(i)}\right\}_{i=1\ldots N}$, $w_k^{(i)} > 0$, $\forall k \geqslant 1$, such that

$$\sum_{i=1}^{N} w_k^{(i)} \varphi_k(x_{0:k}^{(i)}) \underset{N\to\infty}{\rightarrow} \int \varphi_k(x_{0:k}) \pi_k(x_{0:k}) dx_{0:k}, \tag{6}$$

in probability, and where φ_k is any π_k-integrable function. Typically, the target distribution is chosen as $\pi_k(x_{0:k}) = p(x_{0:k}|y_{1:k})$, the posterior probability density function (PDF) of the state vector $x_{0:k}$, conditional to noisy observations $y_{1:k}$.

As in any Bayesian process, the estimation procedure involves two main stages: *prediction*, and *update*. In the prediction stage, the state vector paths $x_{0:k-1}$ are extended using an arbitrary importance distribution $q(\tilde{x}_{0:k}|x_{0:k-1})$, where $\tilde{x}_{0:k} = (x_{0:k-1}, \tilde{x}_k)$. In the update stage, the new weights $w_k^{(i)}$ are evaluated from the measurement likelihood as $w_k^{(i)} \propto w_{k-1}^{(i)} \cdot p(y_k|\tilde{x}_k) \cdot p(\tilde{x}_k|x_{0:k-1}) / q(\tilde{x}_{0:k}|x_{0:k-1})$, where $\sum_{i=1}^{N} w_k^{(i)} = 1$. The most basic PF implementation, the sequential importance sampling particle filter [39], assumes that $p(\tilde{x}_k|x_{0:k-1}) = q(\tilde{x}_{0:k}|x_{0:k-1})$. This procedure generates an empirical representation of the target distribution.

$$\tilde{\pi}_k^N(x_{0:k}) = \sum_{i=1}^{N} w_{0:k}^{(i)} \delta\left(x_{0:k} - \tilde{x}_{0:k}^{(i)}\right). \tag{7}$$

This research considers the implementation of a particle-filtering-based estimator for battery State-of-Charge that provides real-time information about the condition of the energy storage device.

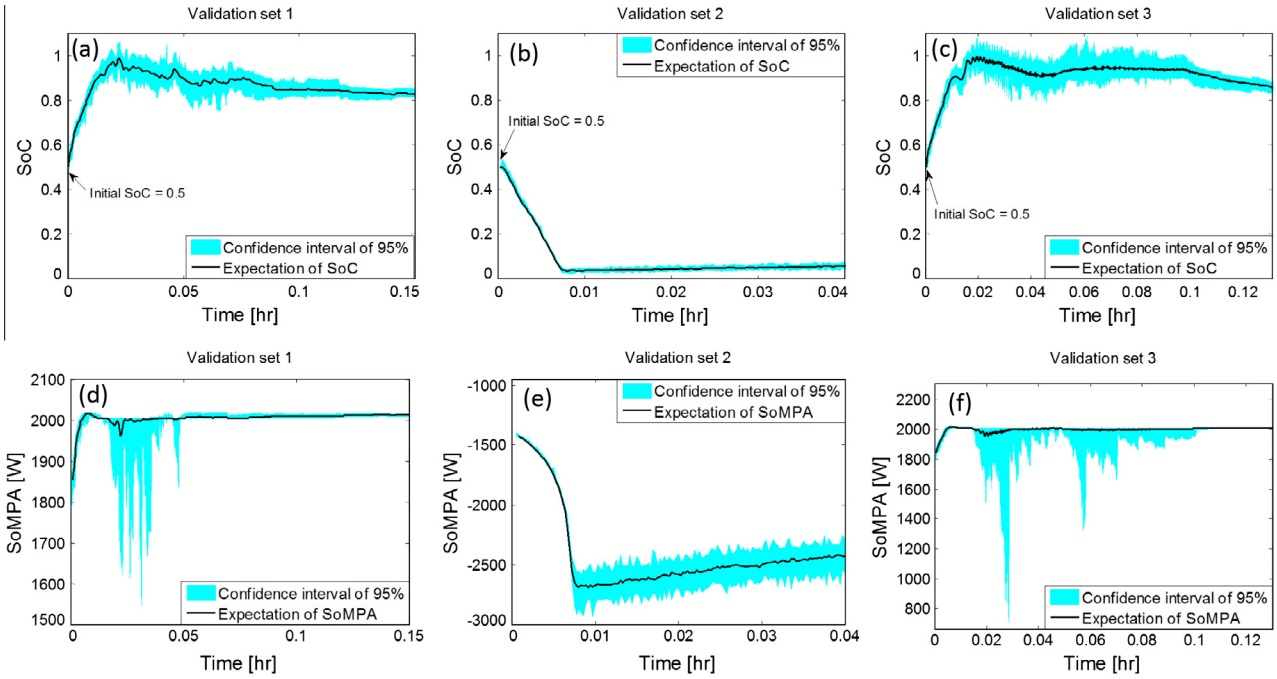

Fig. 12. Convergence process of SoC and SoMPA estimator in the validations sets.

This estimator utilizes state-space model (8) and (9) to define the prior state PDF, and incorporates an improved version of the open-circuit voltage curve (i.e., Eq. (1)) as the system measurement equation [23]. The structure of this state-space model offers a modification to the observation Eq. (9) that incorporates most of the nonlinearities found in Li-Ion open-circuit voltage discharge/charge curves, while simultaneously enabling the implementation of reliable off-line estimation procedures for the estimation of all of its parameters [23].

Eqs. (8) and (9) present the state transition model and the measurement equation, respectively.

$$SoC_k = SoC_{k-1} - \eta \cdot I_{k-1} \cdot T_s \cdot C_n^{-1} + w_k, \tag{8}$$

$$\begin{aligned} V_k(SoC_k, I_k) &= v_L + (v_0 - v_L) \cdot e^{\gamma \cdot (SoC_k - 1)} + \alpha \cdot v_L(SoC_k - 1) + \cdots \\ &\quad + (1-\alpha) v_L (e^{-\beta} - e^{-\beta \cdot \sqrt{SoC_k}}) - I_k \cdot R_{int}(SoC_k, I_k) + \varepsilon_k, \\ V_k(SoC_k, I_k) &= Voc(SoC_k, v_0, v_L, \gamma, \alpha, \beta) - I_k \cdot Fuzzy(SoC_k, I_k) + \varepsilon_k. \end{aligned} \tag{9}$$

In (8) and (9), η is the Coulombic efficiency ($\eta = 1$ and 0.98345 during discharging and charging processes, respectively, for this particular case study), the discharge current I_k (measured in amperes) and the sampling time T_s (measured in seconds) are input variables, and the battery voltage V_k (measured in volts) is the system output. C_n is the battery nominal capacity equal to 34 Ah. Process noise (w_k) and measurement noise (ε_k) are assumed Gaussian. The static function $Fuzzy(\cdot,\cdot)$ represents the fuzzy model structure described in Section 2.1.

The implementation of a particle-filtering-based SoC estimator allows to obtain, in real-time, the information associated with the remnant amount of energy stored in the battery. As the open-circuit voltage curve depends directly on the SoC, this information allows to compute the maximum power that could be extracted/injected from the battery at the present time. Moreover, as particle filtering provides an empirical characterisation of the state PDF, it is possible to measure the uncertainty associated with any nonlinear transformation of the random variable that is being estimated; SoMPA in this case, whose calculation procedure may be considered as the equivalent of a nonlinear transformation of the battery SoC. The latter is a task difficult to achieve using other suboptimal Bayesian SoC estimation approaches such as the extended Kalman filter or the unscented Kalman filter [40]. The procedure that needs to be followed in order to compute the maximum power available at time k (subject to the battery SoC and physical constraints related to the minimum operational voltage and maximum discharge currents) is described in detail in Section 3.

A pseudo-code that helps to illustrate the implementation of PF-based SoC estimation algorithms is presented (based on filtering schemes described in [41–43].

(1) Initialization: $k = 0$

Let us assume that the number of particles used in the algorithm implementation is N, the variance of the Gaussian process noise is R_w, the variance of the measurement Gaussian noise is R_v, and let "x" be the state of the system (in this case, the State of Charge).

- For $i = 1 \ldots N$, draw particles x_0^i from a Gaussian distribution $N(\bar{x}_0, \sigma_0^2)$, where $\bar{x}_0$ is the expectation of the initial SoC condition and σ_0^2 its variance.
- Set initial importance weights $\omega_0^i = \frac{1}{N}$

(2) For $k = 1,2,\ldots$

- Draw N particles $\tilde{x}_k^i$, $i = 1 \ldots N$ using state transition model (8) where w_k is a sample from Gaussian process noise with variance R_w; i.e., generate N particles $\tilde{x}_k^i$ such that $\tilde{x}_k^i = f(x_{k-1}^i, I_k) + w_k^i$
- Calculate the likelihood of each particle as follows:

$$L_k^i = \exp\left(-\frac{1}{2R_v}(y_k - h(\tilde{x}_k^i, I_k))^2\right) \Big/ \sqrt{2\pi R_v}, \tag{10}$$

where y_k is the voltage measurement from de battery bank, and $h(\tilde{x}_k^i, I_k)$ corresponds to the evaluation of particle $\tilde{x}_k^i$ in measurement Eq. (9).

- Compute the importance weights as follows:

$$\tilde{\omega}_k^i = \omega_{k-1}^i \cdot L_k^i.$$

- Normalize the updated importance weights as follows:

$$\omega_k^i = \frac{\tilde{\omega}_k^i}{\sum_{i=1}^{N} \tilde{\omega}_k^i}.$$

(3) Resampling

- Let $\widehat{N}_{eff}(k) = \frac{1}{\sum_{i=1}^{N}(\omega_k^i)^2}$. If $\widehat{N}_{eff} \geqslant N_{thres}$, with N_{thres} a fixed threshold (typically $N_{thres} = 0.85N$), then $x_k^{(i)} \triangleq \tilde{x}_k^i$.
- Otherwise, sample an index $j(i)$ distributed according to the discrete distribution satisfying $P(j(i) = l) = \omega_k^i$, $(l = 1, \ldots, N)$. Set $x_k^{(i)} \triangleq \tilde{x}_k^{j(i)}$ and $\omega_k^i \triangleq N^{-1}$

(4) Output (Conditional Expectation): At each time instant, the particle filtering algorithm generates a PDF estimate for SoC. Therefore the state expectation can be computed as:

$$\hat{x}_k = \sum_{i=1}^{N} \omega_k^i \cdot x_k^i.$$

Steps 1–4 are executed iteratively. It is important to note that this algorithm takes about 1.246 ms to complete one iteration using 100 particles on a Intel(R) Core(TM) i7-4790 CPU @ 3.60 GHz, 8 GB RAM; a fact that facilitates its implementation and execution on real-time devices.

3. Proposed approach for the computation of maximum available power as a function of SoC

The aim of this section is to characterise the relationship between the maximum available power of the battery bank and the state of charge. It is important to note that in real-time applications, where the initial state is typically unknown, or in cases where the system is used for extended time periods, it is not appropriate to determine the SoC only based on the integral of the instantaneous current. In the latter case, the main issue is the numerical errors caused by noisy battery current measurements. Given that we propose to determine the maximum power at instant k based on the information available until instant $k-1$, it is necessary to consider a SoC estimator, which in this case is represented by the implementation of a particle filter algorithm, described in Section 2.2. In the following, the methodology for determining the maximum power available in the battery bank is derived for the charging and discharging processes. The methodology is based on the optimisation problem formulation that uses the battery model described in Section 2.1.

3.1. Formulation of the optimisation problem and KKT conditions

In this section, we derive the analytical solution of the maximum available power based on a simple model of a battery bank. Most of previous research efforts available in the literature present a solution for the SoMPA problem that is based on this simple model, although the theoretical aspects associated to the derivation of this solution are typically omitted. We believe that it is important, for completeness purposes, to include this background as the starting point of our analysis.

For the estimation of the maximum power available for the discharging and charging processes, an optimisation problem is formulated, considering the following battery model with a constant internal resistance (R_{int}):

Discharging process	Charging process	
$V_k = Voc(SoC_k) - R_{int} \cdot I_k$	$V_k = Voc(SoC_k) + R_{int} \cdot I_k$	(11)

where I_k is considered positive on both cases. Then, the power is given by:

Discharging process	Charging process	
$P_k = Voc(SoC_k) \cdot I_k - R_{int} \cdot I_k^2$	$P_k = Voc(SoC_k) \cdot I_k + R_{int} \cdot I_k^2$	(12)

Therefore, for determining the maximum power available, the optimisation problem given by (13) incorporates, as a constraint, the maximum current (I_s) that can be extracted from (or injected to) the battery ($g1$) (120 A, accordingly to manufacturer recommendations [44]), the minimum current ($g2$) and the minimum discharging/charging voltage of the battery ($g3$). Please notice that for the computation of the maximum instantaneous power available it is necessary to solve the optimisation problem shown in (13), which includes hard constraints for battery voltages and currents. These hard constraints are particularly important when the voltage discharge curve reaches its inflection point (at low SoC values); making it impossible to solve solely considering partial derivatives of the Lagrangian.

Discharging process	Charging process	
$Max\ f(I_k) = \left[Voc(SoC_k) \cdot I_k - R_{int} \cdot I_k^2\right]$ s.t. $g1:\ I_k < I_s$ $g2:\ I_k > 0$ $g3:\ V_k < V_k$ where $I_s = 120$ A is the maximum current that can be extracted from the battery and $V_s = 22.4$ V (both values recommended by the manufacturer[a]).	$Max\ f(I_k) = \left[Voc(SoC_k) \cdot I_k + R_{int} \cdot I_k^2\right]$ s.t. $g1:\ I_k < I_s$ $g2:\ I_k > 0$ $g3:\ V_k > V_k$ where $I_s = 120$ A is the maximum current that can be injected from the battery and $V_s = 28.6$ V (both values recommended by the manufacturer).	(13)

[a] Lithium ion batteries model GBS-LFMP40AH.

The optimisation problem shown in (13) can be rewritten as a minimisation problem in order to use the Karush–Kuhn–Tucker conditions. The new optimisation problem is shown in (14).

Discharging process	Charging process	
$Min\ f(I_k) = -\left[Voc(SoC_k) \cdot I_k - R_{int} \cdot I_k^2\right]$ s.t. $g1:\ I_k - I_s < 0$ $g2:\ -I_k < 0$ $g3: I_k + \frac{V_s - Voc(SoC_k)}{R_{int}} < 0$	$Min\ f(I_k) = -\left[Voc(SoC_k) \cdot I_k + R_{int} \cdot I_k^2\right]$ s.t. $g1:\ I_k - I_s < 0$ $g2:\ -I_k < 0$ $g3: I_k - \frac{V_s - Voc(SoC_k)}{R_{int}} < 0$	(14)

The maximum current is obtained, at each SoC value, when the optimisation problem is solved in order to determine the maximum power available. The accuracy of the optimisation problem solutions depends on the complexity of the battery model used.

The optimisation problem (14) is solved using the Karush–Kuhn–Tucker (KKT) conditions [45]. The Lagrangian is given by (15), where $f(I_k)$ are the objective functions shown in (14), $g_i(I_k)$ correspond to the constraints of the optimisation problem, and μ_i are the Lagrange multipliers.

$$L = f(I_k) + \sum_{i=1}^{3} \mu_i \cdot g_i(I_k). \quad (15)$$

Partial derivatives of the Lagrangian (15), with respect to the current I_k, result in KKT conditions given by (16).

$$\nabla f(I_k) + \sum_{i=1}^{3} \mu_i \cdot \nabla g_i(I_k) = 0 \quad \text{and} \quad \mu_i \geqslant 0. \tag{16}$$

The Lagrangian of the optimisation problems described in (14) is stated as follows (notice that the plus sign is for discharging and minus sign is for charging):

$$L(I_k, \mu_1, \mu_2, \mu_3) = -Voc(SoC_k)I_k \pm R_{int}I_k^2 + \mu_1(I_k - I_s) - \mu_2 I_k + \cdots + \mu_3\left(I_k \pm \frac{V_s - Voc(SoC_k)}{R_{int}}\right), \tag{17}$$

where μ_1, μ_2, and μ_3 are the Lagrange multipliers. Then KKT conditions are:

$$\frac{\partial L(I_k, \mu_1, \mu_2, \mu_3)}{\partial I_k} = -Voc(SoC_k) \pm 2R_{int}I_k + \mu_1 - \mu_2 + \mu_3 = 0 \quad \text{and} \quad \mu_1, \mu_2, \mu_3 \geqslant 0. \tag{18}$$

The feasible points (I^*) in these optimisation problem are shown in Table 1.

Analysing the KKT conditions for the discharging and charging processes, the following solutions can be derived, respectively:

$$I^D_{max} = \begin{cases} I_s & \text{if } Voc(SoC_k) > 2R_{int}I_s, \\ -\frac{(V_s - Voc(SoC_k))}{R_{int}} & \text{if } 2V_s > Voc(SoC_k), \end{cases} \tag{19}$$

$$I^C_{max} = \begin{cases} I_s & \text{if } Voc(SoC_k) > -2R_{int}I_s, \\ \frac{(V_s - Voc(SoC_k))}{R_{int}} & \text{if } 2V_s > Voc(SoC_k). \end{cases} \tag{20}$$

Based on experimental results, it was found that the conditions shown in (19) and (20) are always true for the Li-Ion batteries that were tested in this research effort. If we consider the nontrivial solutions provided by (19) and (20) (i.e., those provided in Table 2), we can obtain an expression for the maximum power available that coincides with the one that is typically reported in the literature [8,10,12].

The value of the maximum battery current that is obtained by solving KKT conditions and assuming different SoC values and a simple battery model are shown in Fig. 4a, both for charging and discharging processes. Fig. 4b shows the maximum power available for charging and discharging processes using the aforementioned solutions.

3.2. Solution of the optimisation problem using fuzzy battery models

In Section 2.1, a fuzzy structure was described allowing the battery polarisation resistance to be modelled as a function of both SoC and battery current (during charging and discharging processes). Following the general formulation for the optimisation problem stated in Section 3.1, one can derive the KKT conditions for the extreme point of the optimisation problem that characterises the SoMPA problem, at any arbitrary time k, during discharging and charging processes.

SoMPA for discharging processes:

Considering the fuzzy model of the battery bank described in Section 2.1, that includes the polarisation model depending on the SoC and current level, the optimisation problem for determining the maximum power available, is given by:

$$\begin{aligned} &Max\{Voc(v_0, v_L, \gamma, \alpha, \beta, SoC_k) \cdot I_k - Fuzzy(SoC_k, I_k) \cdot I_k^2\} \\ &\text{s.t.} \\ &g1 : I_k - I_s < 0, \\ &g2 : -I_k < 0, \\ &g3 : I_k + \frac{V_s - Voc(v_0, v_L, \gamma, \alpha, \beta, SoC_k)}{Fuzzy\{SoC_k, I_k\}} < 0, \end{aligned} \tag{21}$$

where SoC is the state of charge estimate at time k, I_k is the discharge current at that time instant, and $I_s = 120$ A, $V_s = 22.4$ V for the battery used in this work (recommended values according to the manufacturer [44]).

SoMPA for charging processes:

The optimisation problem for the charging process is similar to the discharging one (see (21)). Actually, the only differences correspond to the operational ranges and model parameters that are used to characterise the battery charging procedure. Based on this, the optimisation problem is given by:

$$\begin{aligned} &Max\{Voc(v_0, v_L, \gamma, \alpha, \beta, SoC_k) \cdot I_k + Fuzzy(SoC_k, I_k) \cdot I_k^2\} \\ &\text{s.t.} \\ &g1 : I_k - I_s < 0, \\ &g2 : -I_k < 0, \\ &g3 : I_k - \frac{V_s - Voc(v_0, v_L, \gamma, \alpha, \beta, SoC_k)}{Fuzzy\{SoC_k, I_k\}} < 0, \end{aligned} \tag{22}$$

where SoC is the state of charge estimate at time k, I_k is the discharge current at that time instant, and $I_s = 120$ A, $V_s = 28.6$ V for the battery used in this work (recommended values according to the manufacturer [44]).

As this is a nonlinear optimisation problem, iterative search algorithms must be utilised to find the extreme points. Specifically, in this work, the optimisation function *fmincon* and the genetic algorithm toolbox from MATLAB® have been used to solve the aforementioned problem. The extreme point, which in every case is numerically validated as the value where the objective function reaches its minimum, can be computed for every SoC $\in [0,1]$, providing the answer in terms of the maximum discharge current I^D_{max} that can be extracted from the battery during discharge procedures, or directly in terms of the SoMPA. A similar analysis can be made for the case of charging process. In this regard, Fig. 4c shows the solutions of the maximum current for charging (I^C_{max}) and discharging (I^D_{max}) processes, while Fig. 4d illustrates the corresponding SoMPA.

3.3. Particle-filtering-based estimator for maximum available power

Results described in Section 3.2 provide the basis for real-time analysis of the battery performance in terms of the SoMPA, assuming that the battery SoC can be measured on-line. However, as it was mentioned in Section 2.2, that is not the case. Moreover, as the internal resistor depends both on the SoC and the discharge or charge current, any approximation for the battery output power that assumes constant impedance, could incorporate significant biases.

However, the implementation of Bayesian algorithms for real-time estimation of the SoC allows to measure the uncertainty associated with this physical quantity and, as a consequence, to establish probability intervals for the SoMPA. The concept is simple, though effective and efficient.

As particle filtering provides an empirical characterisation of the state PDF, it is possible to measure the uncertainty associated with any nonlinear transformation of the random variable that is being estimated. In this case, the mapping between SoC and SoMPA that results from the optimisation process described in Section 3.2 (see Fig. 4d) can be considered simply a deterministic nonlinear transformation that defines the random variable SoMPA as a function of the random variable SoC. Thus, a particle-filtering-based estimator for the SoMPA can be implemented as two cascaded modules (see Fig. 1). The first module consists of a particle-filtering-based estimator for the SoC estimator, a subject widely studied and well established in the literature [23]. The proposed the SoC, while the second module is a look-up table built on the

basis of the information provided in Fig. 4d. The output of this module consists of an empirical PDF for the SoMPA and therefore, it is possible to extract information related to the expectation of the distribution, with 95% probability intervals and risk measures, among other statistics; see Fig. 1. The precision and accuracy of this empirical PDF is solely related to the number of particles used. This approach can be easily implemented as real-time algorithms running in embedded systems, since most of the existing microprocessors can handle 100 particles in transition equations with two states.

4. Experimental results

4.1. Experimental setup

The experimental system shown in Fig. 5 was designed and implemented at the Power Electronic Lab of the University of Waterloo (Canada). It is designed for charging or discharging a Lithium-Ion battery bank with a given current profile which is regulated using a Digital Signal Processor control platform. The data collected during these charging/discharging cycles has been used to validate the methodology proposed in this work to estimate the battery bank maximum available power.

The system shown in Fig. 5 is based on the experimental system reported in [16]. The methodology to design the current and voltage control loops is similar to that reported in [16]. However, some of the parameters (e.g., nominal power, inductances and switching frequency) have been changed considering that in this work Lithium-Ion batteries are used instead of the lead-acid technology used in [16].

The parameters of the experimental system used in this work are listed in Table 3. Because of completeness, a brief discussion of the experimental rig depicted in Fig. 5 is realised in this section. More information about this system is considered outside the scope of this paper and the interested reader is referred elsewhere [16].

The experimental system used in this work is based on IGBT power electronic devices as shown in Fig. 5a. For battery charging/discharging purposes a constant positive/negative current I_{bat} is regulated by a current control loop [46]. The power generated by discharging the Lithium-Ion battery bank is dissipated in the resistor R (see Fig. 5a). The control loops have been designed using well-known linear control tools as Evan's root locus.

For the control of the experimental system a Digital Signal Processor (DSP) of 16 bit is used (see Table 3). Embedded in this processor are 16 Analogue to Digital converter (ADC) channels with a resolution of 12 bits each, providing a current measurement resolution of ≈±15 mA for the operating range considered in this work. The currents/voltages are measured using high quality Hall effect transducers with an overall accuracy of 0.4% (of the range) for the current transducers and 1% of the range for the voltage transducers. Additionally, in the experimental system an interleaved configuration arrangement is used for the charging/discharging stage. With this topology a considerable reduction in the ripple current circulating through the battery is achieved reducing the overall losses in the system [16,46].

For DSP control purposes a sampling frequency of 10 kHz is used. This high sampling frequency allows the implementation of current/voltage control loops with a high dynamic response and zero steady state error. To avoid an excessive DSP computational burden a separate data acquisition unit based on a USB-connected National Instruments device is interfacing the host-PC to the experimental system. Eight high resolution (14 bits) ADC channels are provided by this device, with a maximum sampling frequency of 6 kHz per channel.

Using both, the DSP and the additional data acquisition unit, high sampling frequencies of the voltage and currents could be achieved. However, as stated before, this work is addressed to study the behaviour of the battery bank in steady-state, low frequency operating range. Therefore, a sampling frequency of 1 Hz is considered appropriate and used to store data in the host PC hard drive.

4.2. Design of experiment

In this section, the data obtained from the experimental system discussed in Section 4.1 is used to identify the parameters of the open circuit voltage versus SoC curve, Simple model, and Fuzzy model.

For this evaluation, the parameters of (1) have been identified using the relaxation test [16] and genetic algorithms [47]. The Voc-versus-SoC curve obtained experimentally for the charging and discharging processes is shown in Fig. 6a. The parameters of the Voc-versus-SoC curve are given in Table 4.

4.3. Performance analysis of the proposed approach

4.3.1. Parameter identification

The data used in the training and validation sets are obtained from battery charging/discharging profiles programmed in the DSP controlling the experimental platform. Note that the effect of temperature was not considered in this work since the experimental setup was allocated in a room with rather constant temperature. The parameters required in the Simple and Fuzzy models are identified using the training sets shown in Fig. 7.

Tables 5 and 6 show, respectively, the parameters of the Simple model and the Fuzzy model, considering both charging and discharging processes. Notice that the parameters σ_x represent the standard deviation in each Gaussian fuzzy sets and the variables a, b represents the parameters in the sigmoidal fuzzy sets. Fig. 6b and c shows the fuzzy sets for discharging and charging processes.

4.3.2. Evaluating of the model performance using the RMSE criterion

In this work, three separated sets are used for validation purposes. These validation sets are not correlated with training sets #1 and #2 (see Fig. 7). A short description of each validation set is given below.

Validation set #1 (Fig. 8): This validation set includes battery discharge profiles obtained at different operating points and has been designed to use instantaneous current levels different from those of the training set #1 (see Fig. 7). Notice that at the beginning of the test, the battery bank is completely charged; i.e., the SoC is almost 100%.

Validation set #2 (Fig. 8): This validation set includes battery charge profiles obtained at different operating points and has been designed to use instantaneous current levels different from those of the training set 2 (see Fig. 7). Notice that at the beginning of the test, the battery bank is completely charged; i.e., the SoC is almost 100%.

Validation set #3 (Fig. 8): This validation emulates the typical operation of a battery bank used in an electric vehicle which have negative and positive currents. The test is started with the battery bank fully charged. At each discharge period, 4.85 AH are extracted from the battery bank. Fig. 9 shows the profile used in this experimental test; please notice that this profile is repeated until the battery bank is fully discharged.

Table 7 shows the performance indices (RMSE) for Simple and Fuzzy models, using the three aforementioned validation sets.

4.3.3. SoC estimator

The particle filtering algorithm previously discussed is implemented for SoC estimation purposes based on Fuzzy model. The performance of the SoC estimator is experimentally validated using validation sets #1, #2 and #3 (see Fig. 8). Notice that for all validation sets, the initial SoC is (arbitrarily) assumed to be 50%. This is assumed to demonstrate the performance of the algorithm when the initial conditions are unknown. The results obtained for each validation set are presented in Fig. 10a–c, d–f and g–i respectively.

Fig. 10a, d and g shows the expectation of the SoC and the confidence interval (of 95%) of the SoC estimate at each sampling time, for validation set #1, validation set #2 and validation set #3, respectively.

On the other hand, Fig. 10b and c shows the estimated SoC PDFs for two different time instants within validation set #1: 0.2 h and 2 h, respectively. Fig. 10e and f shows the estimated SoC PDFs at the same time instants, considering the validation set #2. Finally Fig. 10h and i shows the estimation results for the SoC PDFs computed at time instants 0.14 h and 1.94 h, respectively. Notice that the proposed estimator provides the expectation of the SoC, as well as the confidence interval of this estimation with a 95% confidence level. Moreover, the PDF can be computed at any time instant.

4.3.4. SoMPA estimator

This section focuses on the results obtained with the proposed SoMPA estimator. Notice that for all validation sets, the initial SoC is arbitrarily initialized at 50% of the true value to analyse the impact of erroneous initial conditions. The results for each validation set are as follows.

Fig. 11 shows (i) the expectation of the SoMPA and the confidence interval (of 95%) of the SoMPA estimate at each time instant, and (ii) the PDF of SoMPA of the estimator at some arbitrary time instants for validation sets #1, #2 and #3, respectively. The proposed SoMPA estimator computes the expected value as well as the confidence interval for a given confidence level.

The proposed framework allows us to compute the conditional SoMPA PDF estimate at any arbitrary time instant. Fig. 11b and e depicts the performance of the PF-based PDF estimate at moments in which the filter has converged (uncertainty associated with the estimate is mainly due to measurement noise), whereas Fig. 11c, f, h, and i, depicts a condition in which the filter is updating a biased estimate of the SoMPA (PDFs indicate that the particle population is exploring areas of the state space associated with larger values of the SoMPA). Overall, the robustness of the proposed framework allows to correct for imperfections in the battery model and sensor disturbances in an efficient manner. Notice that in Fig. 11h the PDF support is in the domain of negative SoMPA. However, in Fig. 11i the PDF support is in the positive zone of the SoMPA. This situation happens due to the fact that validation set #3 has both positive and negative currents.

Finally, Fig. 12 shows the convergence process for both SoC and SoMPA estimators in all three validation sets (please be aware that, as mentioned before, for all three validation sets the initial SoC is incorrectly initialised at 50%). In this figure it is possible to notice that both estimation algorithms converge to the true value of the state even when the initial condition is incorrectly set.

5. Conclusions

This paper introduced a novel approach to the estimation of both State of Charge (SoC) and State of Maximum Power Available (SoMPA) in Lithium-Ion batteries. An optimisation problem was formulated for the battery power based on a non-linear dynamic model and the solutions were obtained as functions of SoC. In the battery model, the polarisation resistance was modelled using fuzzy rules that were functions of both SoC and current magnitude. Particle filtering algorithms were used as an online estimation technique, allowing approximation of the probability density functions of the SoC and SoMPA even for non-Gaussian sources of uncertainty. The proposed method for SoMPA estimation was validated using the experimental data obtained from an experimental setup.

As future work, we propose to consider the effects of temperature variations within the fuzzy model for the internal resistance. In those cases, the polarisation resistance will be depend on the SoC, current rate, and temperature. Thus, the fuzzy model should characterise the resistance as a 3-D surface and not simply a curve (as the one shown in Fig. 3). The effects of the SoH on model parameters are also proposed as part of future work.

Acknowledgements

This work has been partially supported by FONDECYT Chile Grants Nrs. 1140774 and 1140775, Advanced Center for Electrical and Electronic Engineering, Basal Project FB0008, and Fondequip EQM130058. The support of the Conicyt scholarship programme for postgraduate studies, is also acknowledged.

References

[1] Soshinskaya M, Crijns-Graus WH, Guerrero JM, Vasquez JC. Microgrids: experiences, barriers and success factors. Renew Sustain Energy Rev 2014;40:659–72.
[2] Ustun TS, Ozansoy C, Zayegh A. Recent developments in microgrids and example cases around the world—a review. Renew Sustain Energy Rev 2011;15:4030–41.
[3] Ubilla K, Jiménez-Estévez GA, Hernádez R, Reyes-Chamorro L, Hernández Irigoyen C, Severino B, et al. Smart microgrids as a solution for rural electrification: ensuring long-term sustainability through cadastre and business models. IEEE Trans Sustain Energy 2014;5(4):1310–8.
[4] Pascual J, Barricarte J, Sanchis P, Marroyo L. Energy management strategy for a renewable-based residential microgrid with generation and demand forecasting. Appl Energy 2015;158:12–25.
[5] Lahiri K, Raghunatha A, Dey S, Panigrahi D. Battery-driven system design: a new frontier in low power design. In: Design automation conference, 2002. Proceedings of ASP-DAC 2002. 7th Asia and South Pacific and the 15th international conference on VLSI design. Proceedings, Bangalore; 2002.
[6] Aditya JP, Ferdowsi M. Comparison of NiMH and Li-ion batteries in automotive applications. In: IEEE vehicle power and propulsion conference (VPPC), Harbin, China; 2008.
[7] Urbain M, Raël S, Davat B, Desprez P. Energetical modelling of lithium-ion battery discharge and relaxation. In: Power electronics specialists conference, 2008. PESC 2008. Rhodes: IEEE; 2008.
[8] Waag W, Fleischer C, Uwe Sauer D. Adaptive on-line prediction of the available power of lithium-ion batteries. J Power Sources 2013;242:548–59.
[9] Xiong R, He H, Sun F, Liu X, Liu Z. Model-based state of charge and peak power capability joint estimation of lithium-ion battery in plug-in hybrid electric vehicles. J Power Sources 2013;229:159–69.
[10] Bhattacharya S, Bauer P. Requirements for charging of an electric vehicle system based on state of power (SoP) and state of energy (SoE). In: 2012 IEEE 7th international power electronics and motion control conference – ECCE Asia, Harbin, China; 2012.
[11] Severino B, Gana F, Palma-Behnke R, Estevez PA, Calderón-Muñoz WR, Orchard ME, et al. Multi-objective optimal design of lithium-ion battery packs based on evolutionary algorithms. J Power Sources 2014;267:288–99.
[12] Fleischer C, Waag W, Bai Z, Uwe Sauer D. Self-learning state-of-available-power prediction for lithium-ion batteries in electrical vehicles. In IEEE vehicle power and propulsion conference, Seoul, Korea; 2012.
[13] Wang Y, Zhang C, Chen Z. A method for joint estimation of state-of-charge and available energy of LiFePO4 batteries. Appl Energy 2014;135:81–7.
[14] Xing Y, He W, Pecht M, Tsui KL. State of charge estimation of lithium-ion batteries using the open-circuit voltage at various ambient temperatures. Appl Energy 2014;113:106–15.
[15] Piller S, Perrin M, Jossen A. Methods for state-of-charge determination and their applications. J Power Sources 2001;96:113–20.
[16] Burgos C, Sáez D, Orchard ME, Cárdenas R. Fuzzy modelling for the state-of-charge estimation of lead-acid batteries. J Power Sources 2015;274:355–66.
[17] Salkind AJ, Fennie C, Singh P, Atwater T, Reisner DE. Determination of state-of-charge and state-of-health of batteries by fuzzy logic methodology. J Power Sources 1999;80:293–300.
[18] Charkhgard M, Farrokhi M. State-of-charge estimation for lithium-ion batteries using neural networks and EKF. IEEE Trans Ind Electron 2010;57:4178–87.

[19] Do DV, Forgez C, El Kadri Benkara K, Friedrich G. Impedance observer for a Li-ion battery. IEEE Trans Veh Technol 2009;58(8):3930–7.
[20] Barillas JK, Li J, Günther C, Danzer MA. A comparative study and validation of state estimation algorithms for Li-ion batteries in battery management systems. Appl Energy 2015;155:455–62.
[21] Wang Y, Zhang C, Chen Z. A method for state-of-charge estimation of Li-ion batteries based on multi-model switching strategy. Appl Energy 2015;137:427–34.
[22] Olivares BE, Cerda Muñoz MA, Orchard ME, Silva JF. Particle-filtering-based prognosis framework for energy storage devices with a statistical characterization of state-of-health regeneration phenomena. IEEE Trans Instrum Meas 2012;62:364–76.
[23] Pola D, Navarrete H, Orchard M, Rabié R, Cerda M, Olivares B, et al. Particle-filtering-based discharge time prognosis for lithium-ion batteries with a statistical characterization of use profiles. IEEE Trans Reliab 2015;64(2):701–9.
[24] energy UDo. PNGV battery test manual, revision 3. DOE/ID-10597; 2001.
[25] Energy UDo. FreedomCAR 42V battery test manual. DOE/ID-II070; 2003.
[26] Kim JH, Jun Lee S, Moon Lee J, Hyung Cho B. A new direct current internal resistance and state of charge relationship for the Li-ion battery pulse power estimation. In: 7th international conference on power electronics, 2007. ICPE '07, Daegu; 2007.
[27] Plett GL. High-performance battery-pack power estimation using a dynamic cell model. IEEE Trans Veh Technol 2004;53(5):1586–93.
[28] Sun F, Xiong R, He H, Li W, Emmanuel Aussems JE. Model-based dynamic multi-parameter method for peak power estimation of lithium-ion batteries. Appl Energy 2012;96:378–86.
[29] Waag W, Fleischer C, Uwe Sauer D. On-line estimation of lithium-ion battery impedance parameters using a novel varied-parameters approach. J Power Sources 2013;237:260–9.
[30] Copetti J, Chenlo F. Lead/acid batteries for photovoltaic applications. Test results and modeling. J Power Sources 1994;47:109–18.
[31] Sun F, Xiong R, He H. Estimation of state-of-charge and state-of-power capability of lithium-ion battery considering varying health conditions. J Power Sources 2014;259:166–76.
[32] Xiong R, Sun F, He H, Duy Nguyen T. A data-driven adaptive state of charge and power capability joint estimator of lithium-ion polymer battery used in electric vehicles. Energy 2013;63:295–308.
[33] Pei L, Zhu C, Wang T, Lu R, Chan C. Online peak power prediction based on a parameter and state estimator for lithium-ion batteries in electric vehicles. Energy 2014;66:766–78.
[34] Wang L, Cheng Y, Zou J. Battery available power prediction of hybrid electric vehicle based on improved dynamic matrix control algorithms. J Power Sources 2014;261:337–47.
[35] Zhang H, Chow M-Y. On-line PHEV battery hysteresis effect dynamics modeling. In: IECON 2010 – 36th annual conference on IEEE Industrial Electronics Society, Glendale, AZ, 2010.
[36] Abu-Sharkh S, Doerffel D. Rapid test and non-linear model characterisation of solid-state lithium-ion batteries. J Power Sources 2004;130:266–74.
[37] Babuska R. Fuzzy modeling for control. United States: KAP; 1998.
[38] Takagi T, Sugeno M. Fuzzy identification of systems and its applications to modeling and control. IEEE Trans Syst, Man Cybernet 2005;15(1):116–32.
[39] Doucet A, de Freitas N, Gordon N. An introduction to sequential Monte Carlo methods. New York: Springer-Verlag; 2001.
[40] Tampier C, Pérez A, Jaramillo F, Quintero V, Orchard ME, Silva JF. Lithium-ion battery end-of-discharge time estimation and prognosis based on Bayesian algorithms and outer feedback correction loops: a comparative analysis. In: Annual conference of the PHM Society 2015, San Diego, CA, USA; 2015.
[41] Gao M, Liu Y, He Z. Battery state of charge online estimation based on particle filter. In: 2011 4th international congress on image and signal processing (CISP), Shanghai; 2011.
[42] Gustafsson F. Particle filter theory and practice with positioning applications. In: Aerospace and electronic systems magazine. IEEE; 2010.
[43] Acuña DE, Orchard ME, Silva JF, Pérez A. Multiple-imputation-particle-filtering for uncertainty characterization in battery state-of-charge estimation problems with missing measurement data: performance analysis and impact on prognostic algorithms. Int J Prog Health Manage 2015.
[44] Zhejiang GBS Energy CO. LTD. <http://www.gbsystem.com/index_en.asp> [accessed 14.07.15].
[45] Eustaquio R, Karas E, Ribeiro A. Constraint qualification for nonlinear programming. In: I Encuentro Regional Argentino Brasileño de Investigación Operativa (ERABIO), Argentina; 2008.
[46] Newlin DS, Ramalakshmi R, Rajasekaran M. A performance comparison of interleaved boost converter and conventional boost converter for renewable energy application. In: 2013 IEEE international conference on green high performance computing (ICGHPC), Nagercoil; 2013.
[47] Man K, Tang K, Kwong S. Genetic algorithms. Springer-Verlag; 1999.